PROTEINS
STRUCTURE ■ FUNCTION ■ BIOINFORMATICS

Crystal structure of human carbonic anhydrase XIII and its complex with the inhibitor acetazolamide

Anna Di Fiore,[1†] Simona Maria Monti,[1†] Mika Hilvo,[2] Seppo Parkkila,[2] Vincenza Romano,[1] Andrea Scaloni,[3] Carlo Pedone,[1] Andrea Scozzafava,[4] Claudiu T. Supuran,[4] and Giuseppina De Simone[1*]

[1] Istituto di Biostrutture e Bioimmagini-CNR, 80134 Naples, Italy

[2] Institute of Medical Technology and School of Medicine, University of Tampere and Tampere University Hospital, University of Tampere, Tampere, Finland

[3] Laboratorio di Proteomica e Spettrometria di Massa, ISPAAM-CNR, 80147 Naples, Italy

[4] Università degli Studi di Firenze, Polo Scientifico, Laboratorio di Chimica Bioinorganica, 50019 Sesto Fiorentino (Florence), Italy

ABSTRACT

The cytosolic isoform XIII is a recently discovered member of the human carbonic anhydrase (hCA, EC 4.2.1.1) family. It is selectively expressed among other tissues in the reproductive organs, where it may control pH and ion balance regulation, ensuring thus proper fertilization conditions. The authors report here the X-ray crystallographic structure of this isozyme in the unbound state and in complex with a classical sulfonamide inhibitor, namely acetazolamide. A detailed comparison of the obtained structural data with those already reported for other CA isozymes provides novel insights into the catalytic properties of the members of this protein family. On the basis of the inhibitory properties of acetazolamide against various cytosolic/transmembrane isoforms and the structural differences detected within the active site of the various CA isoforms, further prospects for the design of isozyme-specific CA inhibitors are here proposed.

Proteins 2009; 74:164–175.

Key words: crystal structure; human carbonic anhydrase XIII; inhibitors.protein-inhibitor complex; rational drug design.

INTRODUCTION

Carbonic anhydrases (CAs) are ubiquitous metalloenzymes, which catalyze the reversible hydration of carbon dioxide to the bicarbonate ion ($CO_2 + H_2O \leftrightarrow HCO_3^- + H^+$). These proteins are present in prokaryotes and eukaryotes, and are encoded by four evolutionarily unrelated gene families: the α-CAs (in vertebrates, bacteria, algae, and cytoplasm of green plants), the β-CAs (predominantly in bacteria, algae and chloroplasts), the γ-CAs (in archaea and some bacteria),[1] and the δ-CAs (in some marine diatoms).[1] Human CAs belong to the alpha class; 15 isoforms are presently known, among which 12 are catalytically active (CAs I–IV, CAs VA–VB, CAs VI–VII, CA IX, and CAs XII–XIV), whereas the CA-related proteins (CARPs) VIII, X, and XI are devoid of any catalytic activity.[1] CA XV is the most recently reported isozyme, which is expressed in a number of species, but is absent in humans and monkeys.[2] CA isozymes widely differ in their kinetic properties, response to inhibitors, pattern of expression in various tissues, and cellular localization. In particular, CAs I, II, III, VII, and XIII reside in cytosol, CAs IV, IX, XII, XIV, and XV are associated with membranes, CAs VA and VB occur in mitochondria, whereas CA VI is secreted.[1–10]

The α-CA isozymes are widely distributed in many tissues and organs in mammals. Since at these sites CAs play a crucial role in various physiological processes, that is, CO_2/HCO_3^- transport between metabolizing tissues and lungs, pH and CO_2 homeostasis, electrolyte secretion, biosynthetic reactions (gluconeogenesis, lipogenesis and ureagenesis), bone resorption, and tumorigenicity,[11–15] they have recently become interesting targets for pharmaceutical research. However, most of the available CA-directed pharmacological agents are still far from being optimal drugs. They present various nondesired side-effects, mainly because of their lack of selectivity for the different CA isozymes.[1] Thus, developing isozyme-specific or, at least, organ-directed CA inhibitors should be highly beneficial in obtaining novel classes of drugs. Prospects for achieving

Abbreviations: AZA, acetazolamide; CA, carbonic anhydrase; CARP, carbonic anhydrase related protein; *d*CA, *dunaliella* carbonic anhydrase; DCP, dichlorophenamide; DMSO, dimethylsulphoxide; DTT, dithiotreitol; DZA, dorzolamide; GST, glutathione-*S*-transferase; hCA, human carbonic anhydrase; IPTG, isopropyl-β-D-thiogalactopyranoside; MZA, methazolamide; NCS, noncrystallographic symmetry; PDB, protein data bank; *p*AMBS, *para*-(amino-methyl)benzensulfonamide; PCR, polymerase chain reaction; PMSF, phenyl-methylsulfonyl fluoride; r.m.s.d., root mean square deviation; TFA, trifluoroacetic acid.

[†]These authors contributed equally to the paper.

Grant sponsor: DeZnIT EU FP6 project.

*Correspondence to: Giuseppina De Simone; Istituto di Biostrutture e Bioimmagini-CNR, via Mezzocannone 16, 80134 Naples, Italy. E-mail: gdesimon@unina.it

Received 4 March 2008; Revised 2 May 2008; Accepted 9 May 2008
Published online 10 July 2008 in Wiley InterScience (www.interscience.wiley.com). DOI: 10.1002/prot.22144

such a goal have not been very optimistic, because of the high similarity observed between various isozymes. However, recently, a plethora of X-ray crystallographic studies on different isozymes and CA-inhibitor complexes have provided a scientific basis for the rational drug design of more selective enzyme inhibitors.[1,14–25] Unfortunately, only the crystal structures of CAs I, II, III, IV, VA, XII, and XIV from different vertebrates have been determined so far.[19,25–30] These isozymes contain an essential Zn^{2+} ion, localized at the bottom of a deep active site cleft, coordinated by three conserved His residues and a water molecule. The Zn^{2+}-bound water is also engaged in H-bond interactions with the hydroxyl moiety of a conserved Thr residue, which in turn is bridged to the carboxylate moiety of a conserved Glu residue. These interactions enhance the nucleophilicity of the Zn^{2+}-bound water molecule, and orient CO_2 toward a favorable location for nucleophilic attack. Since a detailed picture of even the most subtle differences in their active sites should be important for the development of drugs with enhanced selectivity, a complete structural characterization of the remaining CA isozymes is strongly encouraged.

CA XIII is the most recently reported and characterized CA isozyme in humans.[3,31–34] Studies on isozyme distribution in human tissues demonstrated that, similar to CA II, CA XIII occurs in several organs, including thymus, small intestine, and colon. On the other hand, this isozyme is also widely expressed in the testis during all stages of developing sperm cells,[3] while CA II is confined to the mature sperm cells.[3] Contrarily to CA II, CA XIII also occurs in the uterine cervix and some endometrial glands. Since pH and ion balance have to be tightly regulated in reproductive organs to ensure normal fertilization,[3] CA XIII may contribute to reproductive processes by controlling optimal HCO_3^- concentration and pH homeostasis for the maintenance of sperm mobility. This hypothesis could be tested using CA XIII deficient animal models, but unfortunately these models are not yet available. The physiological functions of CA XIII in other tissues and organs still remain to be elucidated.

In this study, we report on the X-ray crystallographic characterization of human CA XIII in the unbound state and in complex with the inhibitor AZA. A detailed comparison of the new structural data with those previously reported for other CA isozymes[1] provided additional insights into the catalytic properties of the members of this protein family. On the basis of the information reported here, novel prospects for the design of isozyme-specific CA inhibitors are proposed.

MATERIALS AND METHODS

Protein expression and purification

The full-length human *CA13* was cloned into the pGEX-4T-1 vector (Amersham Biosciences, Piscataway, NJ), which encodes a GST-fused protein containing a thrombin cleavage site, as reported previously.[31] The full-length human *CA13* cDNA in pOTB7 vector (IMAGE Clone 6083105, Geneservice, Cambridge, UK) was used as template for a PCR reaction, in which the full-length sequence was amplified, and BamHI and XhoI restriction sites were introduced (underlined in primers F1 and R1). The forward primer was 5′-CGC GGA TCC ATG TCG AGG CTC AGC TGG GGA-3′ (F1) and the reverse primer was 5′-CCG CTC GAG TTA ATG GAA AGA GGC TCT CAC-3′ (R1). PCR was performed with Phusion polymerase (Finnzymes, Espoo, Finland) and using PTC 2000 Thermal Cycler (MJ Research, Waltham, MA). The PCR product and the pGEX-4T-1 vector were digested with BamHI and XhoI (New England Biolabs, Herts, UK); then, the PCR product was ligated into the vector by using T4 ligase from Invitrogen (Carlsbad, CA). The recombinant vector encoding GST-CA XIII was transformed into *E. coli* BL21 strain (Amersham Biosciences) and sequence correctness was confirmed as previously reported.[31] Protein expression was carried out in BL21 (DE3) pLysS strain induced with 0.1 m*M* IPTG at 22°C for 16 h. 100 ml pellets were lysed in 5 ml of cold PBS containing 1 mg/mL of lysozyme, aprotinin, leupeptin and pepstatin, 1 m*M* PMSF, 5 m*M* benzamidine, 5 m*M* DTT, 0.05% (v/v) Triton X-100, pH 7.4, following incubation at 25°C, for 30 min. After sonication, the sample was centrifuged at 15000 rpm, at 4°C, for 30 min, and the recombinant protein was purified on 3 mL of GSTrap resin (GE Healthcare), according to manufacturer's suggestions. After treatment with thrombin (GE Healthcare) at 22°C for 16 h, the resulting digest was purified on NHS-activated Sepharose 4 Fast Flow resin (GE Healthcare) preactivated with pAMBS (Sigma) as reported previously.[35,36] Eluted protein was immediately concentrated and loaded on a Superdex 75 (GE Healthcare) equilibrated with 20 m*M* Tris, pH 7.5, 150 m*M* NaCl, 1 m*M* DTT. Highly purified fractions containing hCA XIII were pooled, concentrated to 7 mg/mL and immediately used for crystallization experiments. Protein purity and concentration was evaluated by SDS-PAGE and Bradford method.[37] Protein purity and nature were also verified with a Surveyor HPLC system connected *on-line* with a LCQ DecaXP Ion Trap mass spectrometer (ThermoElectron, USA) equipped with an OPTON electrospray source operating at a needle voltage of 4.2 kV and a temperature of 320°C. Analysis was performed using a 300 Å narrow bore 250 × 2 mm C4 Jupiter column (Phenomenex, Torrance, CA) and applying a gradient of solvent B (0.05% TFA in CH_3CN) on solvent A (0.08% TFA in H_2O) from 30% to 70%, over a period of 40 min. Mass spectra were recorded in the *m/z* 400–2000 range, in positive mode. Multicharge spectra were deconvoluted using the BioMass program implemented in the Bioworks 3.1 package provided by the manufacturer. Mass calibration was performed using UltraMark (Ther-

moElectron) as internal calibrant. Measured mass is reported as average value.

Kinetic and inhibition measurements

Initial rates of CO_2 hydration were measured with an SX.18MV-R Applied Photophysics stopped-flow instrument (Oxford, UK) by the changing pH indicator method.[38] Phenol red at a concentration of 0.2 m*M* was used as indicator in a buffer containing 10 m*M* Hepes, pH 7.5, 0.1*M* Na_2SO_4; CO_2 hydration reaction was measured reading at the absorbance maximum of 557 nm, for a period of 10–100 s. Saturated CO_2 solutions in water at 20°C were used as substrate.[38] Stock solutions of inhibitor (1 m*M*) were prepared in 10–20% (v/v) aqueous DMSO; this organic solvent is not inhibitory at these concentrations. Dilutions up to 0.1 n*M* were done thereafter with water. Prior to assay, inhibitor and enzyme solutions were mixed at 25°C, for 10 min to allow the formation of the enzyme-inhibitor complex. Triplicate experiments were done for each inhibitor concentration, and the values reported are the mean of such results. Inhibition constants were calculated as previously described.[39]

Crystallization and X-ray data collection

The hCA XIII crystals were obtained at 20°C by the hanging drop vapor diffusion method. Drops were prepared by mixing 1 μl of enzyme solution (7 mg/ml) in 20 m*M* Tris-HCl, pH 7.5, 150 m*M* NaCl, 1 m*M* DTT with 1 μl of 30% (w/v) polyethylene glycol 4000, 0.2*M* ammonium acetate, 0.1*M* sodium acetate, pH 4.6, used as precipitant buffer, which were further equilibrated over a well containing 500 μl of precipitant buffer. Crystals appeared in the drops within 24 h and grew in about 1 week to maximum dimensions of 0.2 × 0.3 × 0.3 mm. A complete dataset was collected at 1.55 Å resolution from a single crystal at the temperature of 100 K, using a MAR CCD detector, at the synchrotron source Elettra in Trieste. Prior to cryogenic freezing, crystals were transferred to the precipitant solution with the addition of 15% (w/v) glycerol. Data were processed using the HKL crystallographic data resolution package (Denzo/Scalepack).[40] The crystals belonged to space group $P2_1$ with unit cell dimensions of a = 57.78 Å, b = 58.21 Å, c = 72.12 Å, and β = 92.36°. The Matthews coefficient (V_M = 2.05 Å^3/Da) indicated that the crystallographic asymmetric unit contained two molecules according to a solvent content of 40%.

The hCA XIII-AZA complex was obtained by adding a 5-molar excess of the inhibitor to a 7 mg/mL protein solution in 20 m*M* Tris-HCl, pH 7.5, 150 m*M* sodium chloride, 1 m*M* DTT. Co-crystals of the complex were obtained by the hanging drop vapor diffusion technique at 20°C by using a precipitant solution whose formulation was very similar to that of the native enzyme (30% (w/v) polyethylene glycol 4000, 0.2*M* ammonium acetate, 0.1*M* sodium citrate, pH 5.6). The crystals were then transferred into a fresh precipitant solution also containing 15% (v/v) glycerol prior to flash cooling in liquid N_2. The data were collected by copper rotating anode generator developed by Rigaku and equipped with Rigaku Saturn CCD detector. X-ray data were processed as described above. The crystal symmetry corresponds to $P2_12_12_1$ space group with unit cell dimensions of a = 59.03 Å, b = 81.57 Å, and c = 112.37 Å, with two molecules into the asymmetric unit. Data collection statistics are reported in Table I.

Table I
Data Collection and Refinement Statistics for hCA XIII and hCA XIII-AZA Complex[a]

	CA XIII	CA XIII-AZA
Crystal parameters		
Space group	$P2_1$	$P2_12_12_1$
a (Å)	57.78	59.03
b (Å)	58.21	81.57
c (Å)	72.12	112.37
β (°)	92.36	
Data collection statistics		
Resolution (Å)	20.00–1.55	20.00–2.00
Wavelength (Å)	1.0	1.54
Temperature (K)	100	100
Total reflections	244,442	264,266
Unique reflections	68,200	33,916
Completeness (%)	98.1 (90.3)	90.4 (72.0)
R_{sym}[b]	0.058 (0.258)	0.061 (0.415)
Refinement statistics		
Resolution (Å)	20.00–1.55	20.00–2.00
R_{factor}[c] (%)	16.8	17.8
R_{free}[c] (%)	18.8	21.7
r.m.s.d. from ideal geometry		
Bond lengths (Å)	0.006	0.007
Bond angles (°)	1.4	1.4
Number of protein atoms	4277	4119
Number of inhibitor atoms	–	26
Number of water molecules	777	457
Average B factor (Å^2)	14.41	20.34
Ramachandran analysis		
Most favored (%)	89.4	88.7
Additional allowed (%)	10.4	11.3
Generously allowed (%)	0.2	0.0
Disallowed (%)	0.0	0.0

[a]Values in parentheses refer to the highest resolution shell (1.61–1.55 Å for hCA XIII; 2.07–2.00 Å for hCA XIII-AZA).
[b]$R_{sym} = \Sigma|I_i - \langle I\rangle|/\Sigma I_i$; over all reflections.
[c]$R_{factor} = \Sigma||F_o| - |F_c||/\Sigma|F_o|$; R_{free} calculated with 5% of data withheld from refinement.

Structure determination and refinement

The structure of hCA XIII was solved by the molecular replacement technique using the program AMoRe[41] and the crystallographic structure of hCA II (PDB code 1CA2)[27] as model template. The rotation and translation functions were calculated using data between 15.0 and

Table II
Kinetics and Inhibition of Human CA Isozymes Whose Structure Have Been Solved[a]

Isozyme	k_{cat} (s^{-1})	K_M (m*M*)	k_{cat}/K_M ($M^{-1}s^{-1}$)	K_I (acetazolamide) (n*M*)	Subcellular localization
hCA I[1]	2.0×10^5	4.0	5.0×10^7	250	cytosol
hCA II[1]	1.4×10^6	9.3	1.5×10^8	12	cytosol
hCA III[1]	1.3×10^4	52.0	2.5×10^5	240,000	cytosol
hCA IV[1]	1.1×10^6	21.5	5.1×10^7	74	GPI-anchored
hCA VA[1]	2.9×10^5	10.0	2.9×10^7	63	mitochondria
hCA XII[1]	4.2×10^5	12.0	3.5×10^7	5.7	transmembrane
hCA XIII[31]	$(1.5 \pm 0.1) \times 10^5$	13.8 ± 0.3	$(1.08 \pm 0.05) \times 10^7$	16 ± 0.7	cytosol
hCA XIV[1]	3.1×10^5	7.9	3.9×10^7	41	transmembrane

[a]Kinetic constants for hCA VA and hCA XIV have also been included in the table, even though only the three-dimensional structures of the corresponding murine enzymes are known.

3.5 Å resolution. The one body translation search, using the centered-overlap function (c-o), on the first 50 rotation solutions led to a single solution with a correlation coefficient of 0.215 and an R_{factor} of 0.497. The n-body translation search carried out with the phased-translation function (p-t), by including a PC refinement before each n-body translation search led to find the second molecule. This improved the correlation coefficient and the R_{factor} to 0.442 and 0.426, respectively. Refinement of the structure was performed with CNS[42] and model building was performed with O.[43] Cycles of rigid-body refinement were performed on the model using data between 20.0 and 3.5 Å resolution. At this stage, the resulting R_{factor} and R_{free} were 0.412 and 0.426 respectively. Both molecules in the asymmetric unit were refined without NCS-restraints and thermal B-factors were initially fixed at 20.0 $Å^2$. Many cycles of manual rebuilding and positional and temperature factor refinement were necessary to reduce the crystallographic R_{factor} and R_{free} values (in the 20.00–1.55 Å resolution range) to 0.168 and 0.188, respectively.

The structure of the hCA XIII-AZA complex was solved by molecular replacement using the hCA XIII structure in unbound state as model template. The rotation and translation functions were calculated using data between 15.0 and 3.5 Å resolution. Rigid body, positional and temperature factor refinement in CNS resulted in a final model having $R_{factor} = 0.178$ and $R_{free} = 0.217$. Data refinement statistics for both structures are summarized in Table I. Coordinates and structure factors have been deposited with the PDB (accession code 3D0N and 3CZV for hCA XIII and hCA XIII-AZA, respectively).

RESULTS

Expression, purification, and structure determination of hCA XIII

Recombinant expression of GST-fused human CA XIII was carried out in *Escherichia coli* BL21(DE3) pLysS strain transformed with a pGEX-4T-1 plasmid containing the full-length human *CA13*, following induction with 0.1 m*M* IPTG, for 16 h, at 22°C.[31] hCA XIII was obtained according to the procedure described in the experimental section, upon removal of the fused GST-tag by thrombin treatment. Purified protein was subjected to LC-ESI-MS analysis, which ascertained an apparent mass value (29585.2 ± 1.3 Da) in very good agreement with that expected (29587.28 Da). The latter value took into account the presence of a non-natural dipeptide (Gly-Ser) at protein N-terminus, determining a $\Delta m = +144$ Da with respect to native hCA XIII. Approximately 600 μg of highly purified (>98%) hCA XIII per 100 mL of bacterial culture was achieved; size-exclusion chromatography analysis showed that this protein eluted as a monomer (data not shown).

The CO_2 hydration activity of the recombinant hCA XIII was measured as previously reported.[31] Table II shows the measured kinetic constants, together with those already reported for other human CAs, whose three-dimensional structure is known, that is, CAs I, II, III, IV, and XII. Kinetic constants for hCA VA and hCA XIV have also been included in the table, even though only the three-dimensional structures of the corresponding murine enzymes are known. Inhibition data with acetazolamide, a clinically used CA inhibitor, are also shown. These results demonstrated that the most efficient catalysts for the CO_2 hydration reaction for human isozymes were in order CA II > CA IV ≥ CA I ≥ CA XIV ≥ CA XII ≥ CA VA ≥ CA XIII > CA III. hCA III, a very poor catalyst for CO_2 hydration, was the only isozyme showing lower activity than that measured for hCA XIII. Thus, hCA XIII seems clearly the least active form among the cytosolic CA isozymes with medium activity. On the other hand, the hCA XIII inhibition constant measured for acetazolamide was 16 n*M*. This result showed that the inhibitor binds to hCA XIII with an efficiency similar to that measured for hCAs II, IV, VA, XII, and XIV, but different to that of hCAs I and III (Table II).

To determine the molecular features responsible for these catalytic properties, the high-resolution structure of

Figure 1

Overall fold of hCA XIII: β-strands belonging to the central 10-stranded β-sheet are shown in green (βJ, K39-Y40, βB, A56-N61, βC, F66-F70, βD, Y88-W97, βE, A116-N124, βF, L141-I150, βA, Q173-R175, βH, Y191-G196, βG, V207-L212, βI, R257-A258), helices are shown in red (αA, G12-F19, αB, F20-G25, αD, S130-A135, αE, N154-K168, αF, D180-L185, αG, S219-R227), and additional β-strands in cyan (βa, E32-I33, βb, L47-K50, βc, V78-G81, βd, I108-V109, βe, I216-I218). The catalytic histidines and the zinc ion are shown in ball-and-stick representation. The numbering of amino acid residues and the nomenclature of the secondary structural elements refer to that used for the previously solved structure of hCA II.[27]

the enzyme was solved by X-ray diffraction studies. The enzyme was crystallized in the space group $P2_1$ with two molecules per asymmetric unit, designated **A** and **B**. The structure was solved by molecular replacement using the hCA II structure[27] as starting model and refined with the CNS[42] program. There were no outliers in the Ramachandran plot,[44] and all residues were well defined by the electron density maps. The two independent molecules within the asymmetric unit overlapped quite well; in fact, the superimposition carried out on the Cα positions of all 261 residues led to an r.m.s.d. value of 0.56 Å. For this reason, the following discussion will be conducted only based on one arbitrarily chosen molecule, unless otherwise stated.

hCA XIII overall structure

hCA XIII appeared as a compact globular protein, whose roughly ovoidal shape is approximately 56 × 39 × 40 $Å^3$ in size. Its structure revealed a fold characteristic of other α-CAs, whose three-dimensional structure has been solved,[19,25–30] characterized by a central ten-stranded antiparallel β-sheet surrounded by several helices and additional β-strands (see Fig. 1). As expected on the base of high sequence identity (60%), the hCA XIII three-dimensional model was very similar to that of the best characterized human isozyme, namely hCA II, with all secondary structure elements strictly conserved (Figs. 2 and 3). Accordingly, when superimposing the Ser4-Phe260 hCA XIII Cα atoms with those corresponding in isozyme II, a very low r.m.s.d. was calculated (0.86 Å). However, an accurate analysis revealed a number of small local structural differences between the two enzymes. These differences were localized in the region Ser125-Pro129, as a consequence of the Asp126 insertion, and in the region Tyr51-Ser55 (see Fig. 3); thus, they occurred on the molecular surface, far away from the protein active site.

Active site structure

As observed in the structure of other CA isozymes,[19,25–30] the active site of hCA XIII is located in a large cavity of conical shape, about 15 Å wide and 13 Å long, which reaches the center of the protein molecule. The zinc ion is located at the bottom of this cavity and is ligated with distorted bipyramidal coordination geometry by three histidine residues (His94, His96 and His119), a water molecule and an acetate ion derived from the crystallization buffer (see Fig. 4). The latter coordinates to Zn^{2+} with one oxygen atom, whereas the other one accepts H-bonds both from the Zn^{2+}-bound solvent molecule and the Thr199N atom (see Fig. 4). Binding of this acetate ion is further stabilized by strong van der Waals interactions (distance < 4.5 Å) between its methyl group and Val121, Val143, Leu198, and Trp209 residues. The occurrence of an acetate ion into the enzyme active site was also observed in the structure of hCA II,[46] hCA XII,[25] mCA XIV[30] and *d*CA II from *Dunaliella salina*[47] and was considered to mimic the binding of bicarbonate ion product.

Similarly to that observed for other CA isozymes, hCA XIII active site occurred as a cavity consisting of two distinct portions made of hydrophobic or hydrophilic amino acids. In particular, Val121, Leu198, Ala135, Leu141, Val143, Val207, and Phe131 delimited the hydrophobic region, while Ser62, His64, Asn67, Asp69, Arg91, and Gln92 identified the hydrophilic one. Although refinement was carried out without any NCS-restraints, it is worth noting that all these residues, except His64, adopted an identical conformation within two molecules in the asymmetric unit. As it concerns His64, in molecule **A** it was well defined in the electron density and directed away from the active site, adopting the so called *out* conformation. In molecule **B**, this residue was modeled in two conformations: the first one (more abundant) identical to that observed in molecule **A**, and the second one with the residue pointing toward the active site (*in* conformation).[48,49] The high conformational flexibility of this residue was already reported for other CA isozymes[50] and was associated with its catalytic role as pro-

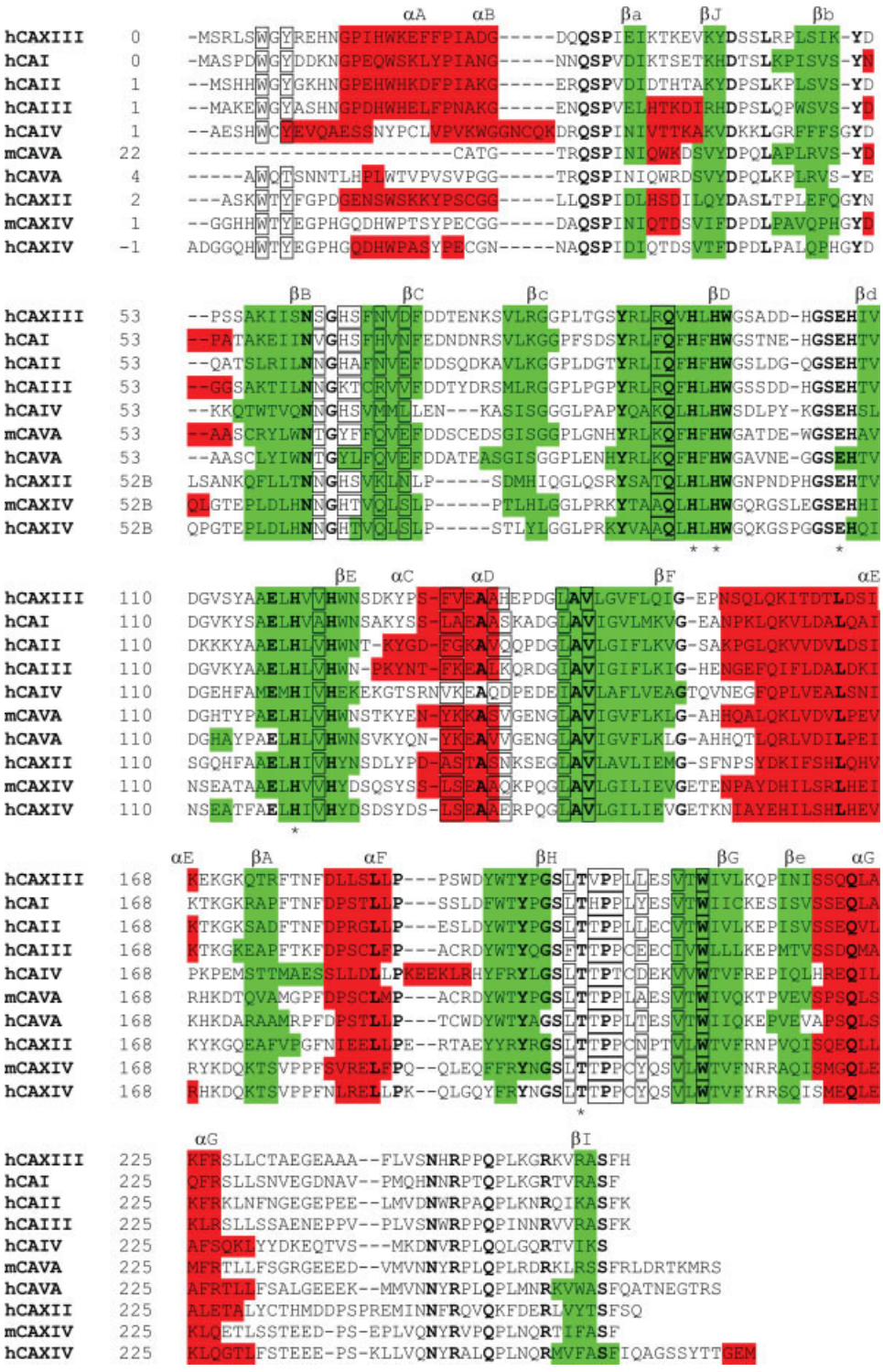

Figure 2

Sequence alignment of α-CAs with known three-dimensional structure. The helix regions are colored in red and β-strand regions in green. Strictly conserved residues are in bold, catalytic triad, Thr199 and Glu106 are starred, while residues delimiting the active site cavity are boxed. Alignments of hCA VA and hCA XIV, whose crystal structures have not been solved yet, were also included. Their secondary structure prediction was carried out by the PSIPRED Protein Structure Prediction Server.[45]

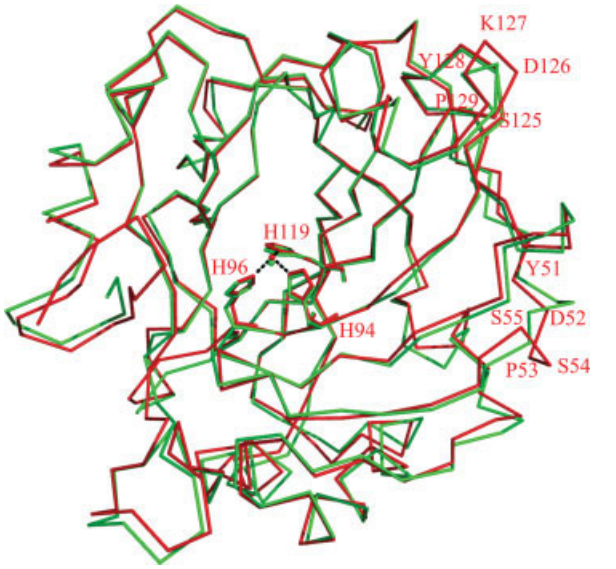

Figure 3

Superposition of the hCA XIII (red) and hCA II (green) Cα trace. The zinc ion and its three histidine ligands are represented in ball and stick.

ton shuttle. The observed preference in the present structure for the *out* conformation is not surprising and is related to the pH used during crystallization.[51] At this pH the positively charged imidazolium group is directed away from the active site in order to minimize its electrostatic repulsion from the positively charged Zn^{2+} ion. The unexpected presence of the *in* conformer, even if in less percentage, may be explained with the presence in the active site of the acetate anion, which partially shields the positive charge of the catalytic zinc.

A careful comparison between hCA XIII and other CAs with known three-dimensional structure revealed a general conservation of the nature and conformation of most of the amino acids present within the active site cavity (see Fig. 2). However, amino acid substitutions at positions 62, 65, 67, 69, 91, 131, 132, 135, 136, 200, and 204 distinguished hCA XIII from the other isozymes. In particular, the occurrence of Ser62 was a unique feature of hCA XIII, with respect to isozymes II-IV, XII, XIV presenting an Asn residue and isozymes I and VA presenting, respectively, a Val and Thr residue at this position. A higher variability occurred at amino acids 67, 69, and 204; in the first case, a residue having an amide-containing side chain was present in isozyme XIII, II, VA, and XIV, whereas a basic or hydrophobic moiety occurred in hCA I, III, XII, and IV, respectively. In the second case, acid (hCA XIII, II, VA), hydrophilic (hCA I, XII, XIV) or hydrophobic (hCA III, IV) residues were similarly present. In the third case, practically all amino acid categories occurred. On the other hand, a positively charged residue (Arg, Lys) at position 91 distinguished hCA XIII, III, IV, and VA from the other isozymes, generally presenting a hydrophobic amino acid at this site. A similar situation also occurred at position 132, where small neutral (hCA XIII, I, II, XII, XIV) or basic (hCA III, IV, VA) amino acids were present. Finally, a Val residue at position 200 clearly distinguished hCA XIII from all other isozymes that always presented a Thr residue at this position (with the exception of hCA I, showing His). Thr200 has been already reported to have an important role for binding of inhibitors to CAs[17,18,52–55]; this nonconservative replacement could determine specific modifications of the isozyme interaction with inhibitor molecules.

Acetazolamide binding to hCA XIII

To detail the binding mode of a classical CA inhibitor to human CA XIII, we determined the crystal structure of the hCA XIII-AZA complex at 2.00 Å resolution. The complex was crystallized in the space group $P2_12_12_1$, with two molecules per asymmetric unit (named **A** and **B**). The structure was solved by molecular replacement using native hCA XIII as starting model and refined with CNS.[42]

A clear electron density for acetazolamide was evident within the active site of each molecule in the asymmetric unit [Fig. 5(A)], which proved nearly identical binding modes. The main protein–inhibitor interactions are schematically depicted in Figure 5(B). According to this fig-

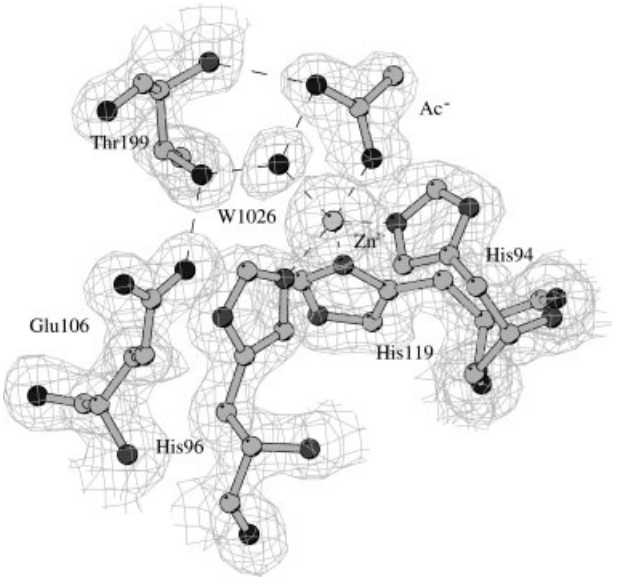

Figure 4

Simulated annealing omit $|2F_o - F_c|$ electron density map relative to the native hCA XIII active site.

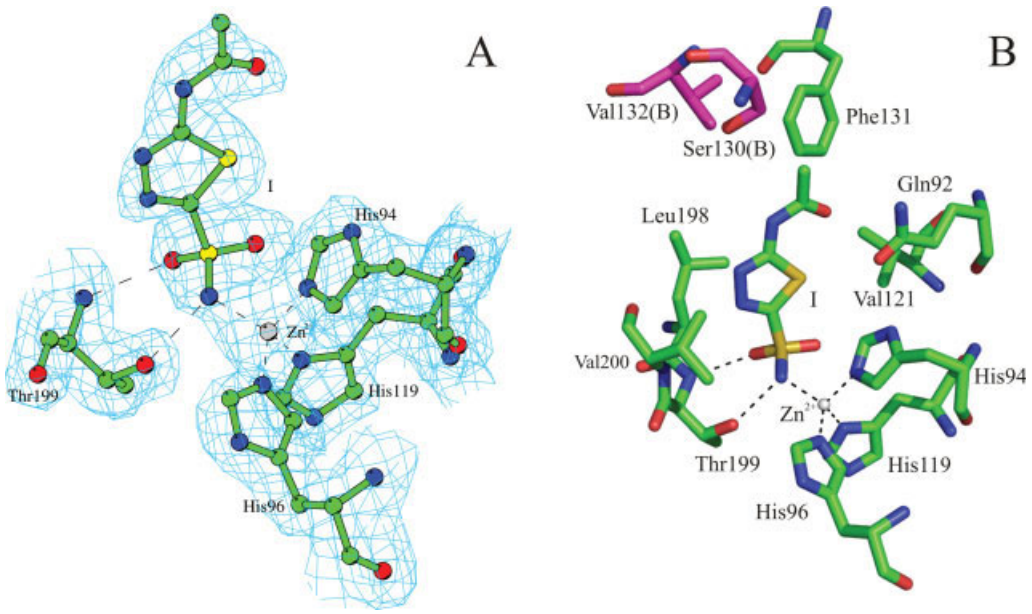

Figure 5

A: Simulated annealing omit $|2F_o - F_c|$ electron density map of the hCA XIII-AZA complex. **B**: The active site region of the hCA XIII-AZA complex, showing residues participating in recognition of the inhibitor molecule. [Color figure can be viewed in the online issue, which is available at www.interscience.wiley.com.]

ure, the ionized sulfonamide N atom of the inhibitor replaces the water molecule and the acetate ion coordinated to Zn^{2+} in the native enzyme, with a Zn^{2+}-N distance of 2.01 Å. Zn^{2+} presents a stable tetrahedral geometry, being also coordinated by the imidazolic nitrogen atoms of His94, His96, and His119. The sulfonamide nitrogen is also involved in a H-bond with the side chain oxygen of Thr199 (2.70 Å), which in turn interacts with the Glu106OE1 atom (2.60 Å). One oxygen of the sulfonamide moiety accepts a hydrogen bond from the backbone NH of Thr199 (2.78 Å), while the other one is located 3.09 Å away from the metal. Several other hydrophobic interactions stabilize the inhibitor within the active site cavity. In particular, the 1,3,4-thiadiazole ring establishes a number of strong van der Waals interactions (distance $<$ 4.5 Å) with residues Gln92, His94, Val121, Leu198, Thr199, and Val200, while the acetamido moiety is stabilized by van der Waals contacts with Gln92, Val121 and Phe131. Van der Waals interactions with residues Ser130 and Val132 of the other molecule in the asymmetric unit also contribute to the stabilization of the inhibitor within the active site [Fig. 5(B)]. It is worth noting that, different from what observed in the native enzyme, the side chain of His64 residue was present only in its *out* conformation as expected on the base of the pH used in the crystallization as well as on the presence of the inhibitor molecule.

As expected, a structural comparison between the hCA XIII-AZA and hCA II-AZA[56–58] complexes revealed that most of the interactions stabilizing the inhibitor within CA active site were conserved in both isozymes. However, the hydrogen bond interactions observed in the hCA II-AZA complex, involving the hydroxyl group of Thr200 and the two N atoms of the thiadiazole ring as well as the Gln92NE2 atom and the carbonyl O of the acetamido moiety, were indeed missing in the hCA XIII-AZA complex. The loss of the first interaction was the obvious consequence of the occurrence of a Val residue at position 200 in isozyme XIII, as discussed in preceding text. The second interaction was lacking as a consequence of the presence of Ser62 in hCA XIII, which replacing the Asn residue occurring in hCA II, was not anymore able to establish interactions with Asn67, which in turn became H-bonded to Gln92. The unique loss of these interactions did not have dramatic consequences on the affinity of acetazolamide for hCA XIII, as suggested by the comparable K_I value reported in this case with respect to that of hCA II (Table II). This finding may indicate that a higher number of chemical interactions has to be perturbed to efficiently discriminate between different isozymes.

DISCUSSION

Although important advances have been recently reported on the catalysis and inhibition of various CAs, an important and still unresolved issue in this research

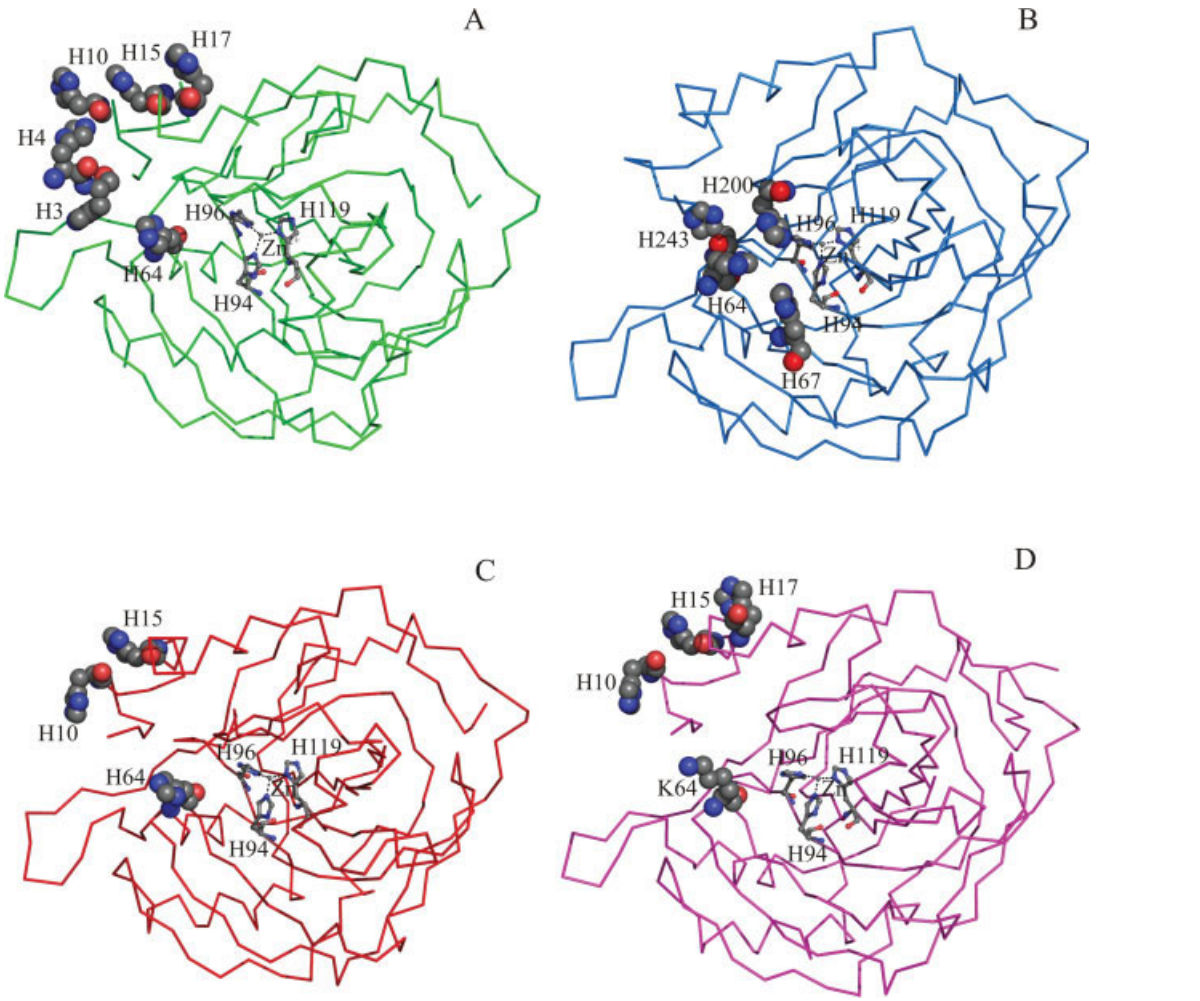

Figure 6

Schematic view of the hCA II (**A**) (PDB code 1CA2),[27] hCA I (**B**) (PDB code 2CAB),[28] hCA XIII (**C**), and hCA III (**D**) (PDB code 1Z93)[26] structures. The zinc ion and its three histidine ligands (H94, H96, and H119) are shown. For each isozyme, the histidine residues participating to the proton-transfer reaction are also reported by PyMOL sphere representation (http://pymol.sourceforge.net/).

field is the complete understanding of the structural determinants of the various vertebrate isozymes contributing to the different catalytic efficiency and response to inhibitors. Based on previous kinetic studies, this protein family consists of very different isozymes including, for example, a perfectly evolved catalyst, CA II,[59] a 10-fold less efficient counterpart, CA I,[60] and a very inefficient isozyme, CA III (see Table II).[61,62] Even greater differences have been observed between isozymes when comparing the K_I values measured for certain clinically used inhibitors. Since a detailed picture of even the most subtle differences in their active sites should be important to investigate these issues, a complete structural characterization of the remaining CA isozymes constitutes an important research priority in this field. Accordingly, we report here the three-dimensional structure of one of the most recently discovered hCA isozymes, namely hCA XIII in the unbound state as well as in complex with acetazolamide.

The kinetic characterization of hCA XIII revealed that the catalytic activity of this isozyme was generally lower than that of other cytosolic hCAs, except hCA III (Table II). As an example, the order of magnitude measured for its efficiency with respect to hCA II was quite surprising, since these two enzymes present a high sequence identity and a high degree of amino acid residues conserved within their active sites. The resolution of hCA XIII three-dimensional structure ensured that no backbone rearrangement was present and the protein fold was quite similar to that of other CAs with solved structure, including hCA II (see Fig. 3). In particular, none of the amino acids differing between hCA XIII and hCA II was

directly implicated in catalysis or binding of the substrate. Thus, the observed differences in their catalytic activities must reside in other structural factors. To identify them, we restricted our structural comparison to the cytosolic isozymes, since membrane and mitochondrial CAs contain other peptide regions that may influence the catalytic activity, thus limiting our rationalization. The generally accepted catalytic mechanism for physiological CO_2 hydration involves the nucleophilic attack of the Zn^{2+}-bound hydroxide to the substrate, optimally activated and oriented in the hydrophobic pocket of the CA active site.[59,63,64] Bicarbonate formed in this way is then replaced by a water molecule, with generation of the catalytically inactive form of the enzyme EZn^{2+}-OH_2. To regenerate the catalytically-active form, a proton-transfer reaction must occur from the Zn^{2+}-bound water within the enzyme active site toward the external medium. This reaction represents the rate-limiting step in catalysis, and may be assisted either by His64, a proton shuttle residue present in the active-site of several α-CAs isoforms, or by buffers within the medium.[65] In the case of hCA II, the highest catalytic efficiency observed was associated with a unique histidine cluster within the enzyme active site, made of His64, His3, His4, His10, His15, and His17 [Fig. 6(A)].[66] This cluster extends from the interior of the active site to its entrance and, finally, to the surface of the protein. It was suggested that this structural motif constitutes an appropriate "channel" for efficiently assisting transfer of protons from the active site to the reaction medium.[66] Its importance for catalytic efficiency was supported by other kinetic/structural studies on a medium-activity isozyme, namely hCA I.[60] In this case, the reduced catalytic efficiency well paralleled with a cluster that was not well defined in the enzyme structure [Fig. 6(B)], as a result of some histidine substitutions between isozymes I and II and a number of additional residues within the active site, namely His67, His200, and His243, placed at bifurcating positions and buried enough to assist only partially proton transfer.

The data reported in this study definitively confirm the role of the histidine cluster on the enzyme catalytic efficiency. In fact, the lower catalytic efficiency measured for hCA XIII, with respect to hCA II and hCA I, corresponded to an isozyme structure where the histidine cluster was not at all present [Fig. 6(C)]. In fact, apart from His64, no other histidine residue was present in the channel connecting the active site to the protein surface. The external residues His10 and His15 were placed too distant to ensure a proper proton transfer. The poorest activity measured for hCA III was in line with these observations too. For this isoform, His64, present in all isozymes and acting as the initial proton transfer moiety, was replaced by a Lys residue [Fig. 6(D)]. Also in this case, His10, His15, and His17, confined on the protein surface, were noninfluent for a proper proton transfer.

A detailed comparative analysis of the acetazolamide inhibition constants for various CAs (see Table II) revealed that human isozyme XIII bound acetazolamide with an efficiency similar to that of hCA II, IV, VA, XII, XIV, and significantly higher than that measured for hCA I and III (see Table II). A similar inhibitory trend was observed with other classical sulfonamide inhibitors (MZA, DCP, DZA) using murine CA XIII, hCA I and hCA II[33]; contrarily, a higher selectivity toward murine CA XIII was detected for sulfanilyl-sulfonamide type of inhibitors.[33] To identify the molecular features responsible of such behavior, a careful structural comparison between hCA XIII and the other CAs, with known three-dimensional structure, has been performed revealing a general conservation of the nature and conformation of most of the amino acids present within the active site cavity (Trp5, Tyr7, Gln92, Val121, Leu141, Val143, Leu198, Pro201, Pro202, Val207, and Trp209) (see Fig. 2). The amino acid substitutions (at position 62, 65, 67, 69, 91, 131, 132, 135, 136, 200, and 204) distinguishing hCA XIII from other CAs do not justify individually why this isozyme binds acetazolamide with an affinity comparable to that of hCA II, IV, VA, XII, XIV, and higher of that of hCA I and III. Therefore, rather than a specific binding to one of these amino acids, a multiple combination of interactions/repulsions involving all of them has to be evoked to finally explain the inhibition constants measured for each isozyme. Support to this hypothesis comes from the observation that, even though the structural comparison of hCA XIII-AZA and hCA II-AZA complexes reveals the lack of important hydrogen bond interactions in the first one, the inhibitor shows a comparable binding affinity toward both isozymes (see Table II). On the basis of these observations, we can conclude that a comparative evaluation of all possible differences between the active site of all isozymes has to be carefully evaluated to identify structural determinants to be considered in multiple combinations for an optimal design of isozyme-specific CA inhibitors. These compounds will have to simultaneously satisfy eventual steric hindrance, H-bonding and van der Waals interaction/repulsion criteria, for achieving isozyme selectivity.

ACKNOWLEDGMENTS

The authors thank Sincrotrone Trieste CNR/Elettra facility for giving the opportunity to collect data at the Crystallographic Beamline.

REFERENCES

1. Supuran CT. Carbonic anhydrases: novel therapeutic applications for inhibitors and activators. Nat Rev Drug Discov 2008;7:168–181.
2. Hilvo M, Tolvanen M, Clark A, Shen B, Shah GN, Waheed A, Halmi P, Hänninen M, Hämäläinen JM, Vihinen M, Sly WS, Parkkila S. Characterization of CA XV, a new GPI-anchored form of carbonic anhydrase. Biochem J 2005;392:83–92.

3. Lehtonen JM, Shen B, Vihinen M, Casini A, Scozzafava A, Supuran CT, Parkkila A-K, Saarnio J, Kivelä AJ, Waheed A, Sly WS Parkkila S. Characterization of CA XIII, a novel member of the carbonic anhydrase isozyme family. J Biol Chem 2004;279:2719–2727.
4. Pastorekova S, Parkkila S, Pastorek J, Supuran CT. Carbonic anhydrases: current state of the art, therapeutic applications and future prospects. J Enzyme Inhib Med Chem 2004;19:199–229.
5. Scozzafava A, Mastrolorenzo A, Supuran CT. Modulation of carbonic anhydrase activity and its applications in therapy. Exp Opin Ther Pat 2004;14:667–702.
6. Scozzafava A, Mastrolorenzo A, Supuran CT. Carbonic anhydrase inhibitors and activators and their use in therapy. Exp Opin Ther Pat 2006;16:1627–1664.
7. Supuran CT, Scozzafava A, Casini A. Carbonic anhydrase inhibitors. Med Res Rev 2003;23:146–189.
8. Supuran CT. Carbonic anhydrases as drug targets—an overview. Curr Top Med Chem 2007;7:825–833.
9. Supuran CT, Scozzafava A. Carbonic anhydrases as targets for medicinal chemistry. Bioorg Med Chem 2007;15:4336–4350.
10. Winum J-Y, Scozzafava A, Montero J-L, Supuran CT. New zinc binding motifs in the design of selective carbonic anhydrase inhibitors. Mini-Rev Med Chem 2006;6:921–936.
11. Hilvo M, Rafajová M, Pastoreková S, Pastorek J, Parkkila S. Expression of carbonic anhydrase IX in mouse tissues. J Histochem Cytochem 2004;52:1313–1322.
12. Kaunisto K, Parkkila S, Rajaniemi H, Waheed A, Grubb J, Sly WS. Carbonic anhydrase XIV: luminal expression suggests key role in renal acidification. Kidney Int 2002;61:2111–2118.
13. Kyllönen MS, Parkkila S, Rajaniemi H, Waheed A, Grubb JH, Shah GN, Sly WS, Kaunisto K. Localization of carbonic anhydrase XII to the basolateral membrane of H^+-secreting cells of mouse and rat kidney. J Histochem Cytochem 2003;51:1217–1224.
14. Menchise V, De Simone G. Alterio V. Di Fiore A, Pedone C, Scozzafava A, Supuran CT. Carbonic anhydrase inhibitors: stacking with Phe131 determines active site binding region of inhibitors as exemplified by the X-ray crystal structure of a membrane-impermeant antitumor sulfonamide complexed with isozyme II. J Med Chem 2005;48:5721–5727.
15. Weber A, Casini A, Heine A, Kuhn D, Supuran CT, Scozzafava A, Klebe G. Unexpected nanomolar inhibition of carbonic anhydrase by COX-2-selective celecoxib: new pharmacological opportunities due to related binding site recognition. J Med Chem 2004;47:550–557.
16. Abbate F, Casini A, Owa T, Scozzafava A, Supuran CT. Carbonic anhydrase inhibitors: E7070, a sulfonamide anticancer agent, potently inhibits cytosolic isozymes I and II, and transmembrane, tumor-associated isozyme IX. Bioorg Med Chem Lett 2004;14:217–223.
17. Alterio V, Vitale RM, Monti SM, Pedone C, Scozzafava A, Cecchi A, De Simone G, Supuran CT. Carbonic anhydrase inhibitors: X-ray and molecular modeling study for the interaction of a fluorescent antitumor sulfonamide with isozyme II and IX. J Am Chem Soc 2006;128:8329–8335.
18. Alterio V, De Simone G, Monti SM, Scozzafava A, Supuran CT. Carbonic anhydrase inhibitors: inhibition of human, bacterial, and archaeal isozymes with benzene-1,3-disulfonamides—solution and crystallographic studies. Bioorg Med Chem Lett 2007;17:4201–4207.
19. Boriack-Sjodin PA, Heck RW, Laipis PJ, Silverman DN, Christianson DW. Structure determination of murine mitochondrial carbonic anhydrase V at 2.45-A resolution: implications for catalytic proton transfer and inhibitor design. Proc Natl Acad Sci USA 1995; 92:10949–10953.
20. Casini A, Antel J, Abbate F, Scozzafava A, David S, Waldeck H, Schafer S, Supuran CT. Carbonic anhydrase inhibitors: SAR and X-ray crystallographic study for the interaction of sugar sulfamates/sulfamides with isozymes I. II and IV. Bioorg Med Chem Lett 2003;13:841–845.
21. De Simone G, Di Fiore A, Menchise V, Pedone C, Antel J, Casini A, Scozzafava A, Wurl M, Supuran CT. Carbonic anhydrase inhibitors. Zonisamide is an effective inhibitor of the cytosolic isozyme II and mitochondrial isozyme V: solution and X-ray crystallographic studies. Bioorg Med Chem Lett 2005;15:2315–2320.
22. Kim C-Y, Chang JS, Doyon JB, Baird TT, Fierke CA, Jain A, Christianson DW. Contribution of fluorine to protein-ligand affinity in the binding of fluoroaromatic inhibitors to carbonic anhydrase II. J Am Chem Soc 2000;122:12125–12134.
23. Smith GM, Alexander RS, Christianson DW, McKeever BM, Ponticello GS, Springer JP, Randall WC, Baldwin JJ, Habecker CN. Positions of His-64 and a bound water in human carbonic anhydrase II upon binding three structurally related inhibitors. Protein Sci 1994;3:118–125.
24. Stams T, Chen Y, Boriack-Sjodin PA, Hurt JD, Liao J, May JA, Dean T, Laipis P, Silverman DN, Christianson DW. Structures of murine carbonic anhydrase IV and human carbonic anhydrase II complexed with brinzolamide: molecular basis of isozyme-drug discrimination. Prot Sci 1998;7:556–563.
25. Whittington DA, Waheed A, Ulmasov B, Shah GN, Grubb JH, Sly WS, Christianson DW. Crystal structure of the dimeric extracellular domain of human carbonic anhydrase XII, a bitopic membrane protein overexpressed in certain cancer tumor cells. Proc Natl Acad Sci USA 2001;98:9545–9550.
26. Duda DM, Tu C, Fisher SZ, An H, Yoshioka C, Govindasamy L, Laipis PJ, Agbandje-McKenna M, Silverman DN, McKenna R. Human carbonic anhydrase III: structural and kinetic study of catalysis and proton transfer. Biochemistry 2005;44:10046–10053.
27. Eriksson AE, Jones TA, Liljas A. Refined structure of human carbonic anhydrase II at 2.0 Å resolution. Proteins 1988;4:274–282.
28. Kannan KK, Ramanadham M, Jones TA. Structure, refinement, and function of carbonic anhydrase isozymes: refinement of human carbonic anhydrase I. Ann N Y Acad Sci 1984;429:49–60.
29. Stams T, Nair SK, Okuyama T, Waheed A, Sly WS, Christianson DW. Crystal structure of the secretory form of membrane-associated human carbonic anhydrase IV at 2.8 Å resolution. Proc Natl Acad Sci USA 1996;93:13589–13594.
30. Whittington DA, Grubb JH, Waheed A, Shah GN, Sly WS, Christianson DW. Expression, assay, and structure of the extracellular domain of murine carbonic anhydrase XIV: implications for selective inhibition of membrane-associated isozymes. J Biol Chem 2004; 279:7223–7228.
31. Hilvo M, Innocenti A, Monti SM, De Simone G, Supuran CT, Parkkila S. Recent advances in research on the most novel carbonic anhydrases. CA XIII and XV Curr Pharm Des 2008;14:672–678.
32. Innocenti A, Lehtonen JM, Parkkila S, Scozzafava A, Supuran CT. Carbonic anhydrase inhibitors. Inhibition of the newly isolated murine isozyme XIII with anions. Bioorg Med Chem Lett 2004;14: 5435–5439.
33. Lehtonen JM, Parkkila S, Vullo D, Casini A, Scozzafava A, Supuran CT. Carbonic anhydrase inhibitors. Inhibition of cytosolic isozyme XIII with aromatic and heterocyclic sulfonamides: a novel target for the drug design. Bioorg Med Chem Lett 2004;14:3757–3762.
34. Parkkila S, Vullo D, Puccetti L, Parkkila A-K, Scozzafava A, Supuran CT. Carbonic anhydrase activators: activation of isozyme XIII with amino acids and amines. Bioorg Med Chem Lett 2006;16:3955–3959.
35. Heck RW, Tanhauser SM, Manda R, Tu CK, Laipis PJ, Silverman DN. Catalytic properties of mouse carbonic anhydrase V. J Biol Chem 1994;269:24742–24746.
36. Khalifah RG, Strader DJ, Bryant SH, Gigson SM. Carbon-13 nuclear magnetic resonance probe of active-site ionizations in human carbonic anhydrase B. Biochemistry 1977;16:2241–2247.
37. Bradford M. A rapid and sensitive method for the quantitation of microgram quantities of protein utilizing the principle of protein-dye binding. Anal Biochem 1976;72:248–253.
38. Khalifah RG. The carbon dioxide hydration activity of carbonic anhydrase. J Biol Chem 1971;246:2561–2573.

39. Scozzafava A, Menabuoni L, Mincione F, Briganti F, Mincione G, Supuran CT. Carbonic anhydrase inhibitors. Perfluoroalkyl/arylsubstituted derivatives of aromatic/heterocyclic sulfonamides as topical intraocular pressure lowering agents with prolonged duration of action. J Med Chem 2000;43:4542–4551.
40. Otwinowski Z, Minor W. Processing of X-ray diffraction data collected in oscillation mode. Methods Enzymol 1997;276:307–326.
41. Navaza J. AMoRe: an automated package for molecular replacement. Acta Crystallogr Sect A 1994;50:157–163.
42. Brünger AT, Adams PD, Clore GM, De Lano WL, Gros P, Grosse-Kunstleve RW, Jiang JS, Kuszewski J, Nilges M, Pannu NS, Read RJ, Rice LM, Simonson T, Warren GL. Crystallography & NMR system: a new software suite for macromolecular structure determination. Acta Crystallogr Sect D 1998;54:905–921.
43. Jones TA, Zou JY, Cowan SW, Kjeldgaard M. Improved methods for building protein models in electron density maps and the location of errors in these models. Acta Crystallogr Sect A 1991;47:110–119.
44. Laskowski RA, MacArthur MW, Moss DS, Thornton JM. PROCHECK: a program to check the stereochemical quality of protein structures. J Appl Crystallogr 1993;26:283–291.
45. McGuffin LJ, Bryson K, Jones DT. The PSIPRED protein structure prediction server. Bioinformatics 2000;16:404–405.
46. Håkansson K, Briand C, Zaitsev V, Xue Y, Liljas A. Wild-type and E106Q mutant carbonic anhydrase complexed with acetate. Acta Crystallogr Sect D 1994;50:101–104.
47. Premkumar L, Greenblatt HM, Bageshwar UK, Savchenko T, Gokhman I, Sussman JL, Zamir A. Three-dimensional structure of a halotolerant algal carbonic anhydrase predicts halotolerance of a mammalian homolog. Proc Natl Acad Sci USA 2005;102:7493–7498.
48. Håkansson K, Carlsson M, Svensson LA, Liljas A. Structure of native and apo carbonic anhydrase II and structure of some of its anion-ligand complexes. J Mol Biol 1992;227:1192–1204.
49. Maupin CM, Voth GA. Preferred orientations of His64 in human carbonic anhydrase II. Biochemistry 2007;46:2938–47.
50. Fisher Z, Prada JAH, Tu C, Duda D, Yoshioka C, An HQ, Govindasamy L, Silverman DN, McKenna R. Structural and kinetic characterization of active-site histidine as a proton shuttle in catalysis by human carbonic anhydrase II. Biochemistry 2005;44:1097–1105.
51. Nair SK, Christainson DW. Unexpected pH-dependent conformation of His64, the Proton Shuttle of Carbonic Anhydrase II. J Am Chem Soc 1991;113:9455–9458.
52. De Simone G, Vitale RM, Di Fiore A, Pedone C, Scozzafava A, Montero J-L, Winum J-Y, Supuran CT. Carbonic anhydrase inhibitors: hypoxia-activatable sulfonamides incorporating disulfide bonds that target the tumor-associated isoform IX. J Med Chem 2006;49: 5544–5551.
53. Di Fiore A, De Simone G, Menchise V, Pedone C, Casini A, Scozzafava A, Supuran C. T. Carbonic anhydrase inhibitors: X-ray crystal structure of a benzenesulfonamide strong CA II and CA IX inhibitor bearing a pentafluorophenylaminothioureido tail in complex with isozyme II. Bioorg Med Chem Lett 2005;15:1937–1942.
54. Di Fiore A, Pedone C, D'Ambrosio K, Scozzafava A, De Simone G, Supuran CT. Carbonic anhydrase inhibitors: Valdecoxib binds to a different active site region of the human isoform II as compared to the structurally related cyclooxygenase II selective' inhibitor celecoxib. Bioorg Med Chem Lett 2006;16:437–442.
55. Winum J-Y, Temperini C, El Cheikh K, Innocenti A, Vullo D, Ciattini S, Montero J-L, Scozzafava A, Supuran CT. Carbonic anhydrase inhibitors: clash with Ala65 as a means for designing inhibitors with low affinity for the ubiquitous isozyme II, exemplified by the crystal structure of the topiramate sulfamide analogue. J Med Chem 2006;49:7024–7031.
56. Huang CC, Lesburg CA, Kiefer LL, Fierke CA, Christianson DW. Reversal of the hydrogen bond to zinc ligand histidine-119 dramatically diminishes catalysis and enhances metal equilibration kinetics in carbonic anhydrase II. Biochemistry 1996;35:3439–3446.
57. Nair SK, Krebs JF, Christianson DW, Fierke CA. Structural basis of inhibitor affinity to variants of human carbonic anhydrase II. Biochemistry 1995;34:3981–3989.
58. Vidgren J, Liljas A, Walker NP. Refined structure of the acetazolamide complex of human carbonic anhydrase II at 1.9 Å. Int J Biol Macromol 1990;12:342–344.
59. Silverman DN, Lindskog S. The catalytic mechanism of carbonic anhydrase: implications of a rate-limiting protolysis of water. Acc Chem Res 1988;21:30–36.
60. Lindskog S, Behravan G, Engstrand C, Forsman C, Jonsson BH, Liang Z, Ren X, Xue Y. Structure, function relations in human carbonic anhydrase II as studied by site-directed mutagenesis. In: Botre' F, Gros G, Storey BT, editors. Carbonic anhydrases from biochemistry and genetics to physiology and clinical medicine. Weinheim: Verlag Chemie; 1991. pp 1–13.
61. Engberg P, Millqvist E, Pohl G, Lindskog S. Purification and some properties of carbonic anhydrase from bovine skeletal muscle. Arch Biochem Biophys 1985;241:628–638.
62. Paranawithana SR, Tu C, Jewell DA, Laipis PJ, Silverman DN. Catalytic enhancement of carbonic anhydrase III by introduction of histidine 64 as proton shuttle. In: Botre' F, Gros G, Storey BT, editors. Carbonic anhydrases from biochemistry and genetics to physiology and clinical medicine. Weinheim: Verlag Chemie; 1991. pp 14–21.
63. Christianson DW, Fierke CA. Carbonic anhydrase: evolution of the zinc binding site by nature and by design. Acc Chem Res 1996;29: 331–339.
64. Lindskog S, Liljas A. Carbonic anhydrase. Structure and catalytic mechanism. Roum Chem Q Re V 1994;2:243–258.
65. Roy A, Taraphder S. Proton transfer pathways in the mutant His-64-Ala of human Carbonic Anhydrase II. Biopolymers 2006;82:623–630.
66. Briganti F, Mangani S, Orioli P, Scozzafava A, Vernaglione G, Supuran CT. Carbonic anhydrase activators: X-ray crystallographic and spectroscopic investigations for the interaction of isozymes I and II with histamine. Biochemistry 1997;36:10384–10392.